Chemical Engineering Journal 458 (2023) 141498

Contents lists available at ScienceDirect

Chemical Engineering Journal

journal homepage: www.elsevier.com/locate/cej

Gold recovery from E-waste using freestanding nanopapers of cellulose and ionic covalent organic frameworks

Qinqin Xu [a], Xing-Hao Du [a], Dan Luo [a], Maria Strømme [b], Qian-Feng Zhang [a], Chao Xu [a,b,*]

[a] Institute of Molecular Engineering and Applied Chemistry, Anhui University of Technology, Ma'anshan 243002, PR China
[b] Division of Nanotechnology and Functional Materials, Department of Materials Science and Engineering, Ångström Laboratory, Uppsala University, Uppsala SE-75121, Sweden

ARTICLE INFO

Keywords:
E-waste
Precious metal recovery
Covalent organic frameworks
Cellulose fibers
Freestanding membranes

ABSTRACT

The ever-increasing production of electronic devices generates a huge amount of electronic waste (E-waste). Therefore, there is an urgent need for advanced recycling technology for E-waste that provides both economic and environmental benefits. Herein, we describe the preparation of flexible, freestanding CF-COF nanopapers consisting of cellulose fibers (CFs) and guanidinium-based ionic covalent organic framework (COF) that can be used for recovering gold from E-waste leaching solutions via a membrane separation technique. Due to the synergetic effects of physical adsorption, ion exchange and chemical reduction, the COF has an extremely high capture capacity (up to 1,794 mg of Au per gram of COF), is highly selective and has fast kinetics for adsorbing trace amounts of $[AuCl_4]^-$ in aqueous solution. The high COF loadings (~50 wt%) and hierarchical porosity of the CF-COF nanopapers resulted in excellent performance when capturing gold species from the E-waste leaching solution. This study provides new possibilities for developing sustainable membrane materials, and highly efficient and cost-effective techniques for the recovery of precious metals from E-waste.

1. Introduction

E-waste is becoming one of the faster growing waste streams because of the increased consumption of various electronics such as smart phones, computers, and displays [1–3]. However, with the proper technology, E-waste could become a sustainable resource because it contains abundant valuable metals [4,5]. The UN has reported that at least $47 billion worth of gold, copper and other precious metals are dumped every year in E-waste [6]. Therefore, there is an increasing need for precious metal recovery from E-waste, also called urban mining [7], in order to achieve a circular economy and a more sustainable society. However, the lack of efficient, environmentally friendly recovery technology has significantly hampered the development of urban mining [8–10]. While pyrometallurgy, where metals are melted at high temperatures and then recovered, is a traditional and widely used method for recycling E-waste, the process is energy-intensive, lacks selectivity, and produces hazardous fumes containing heavy metals [11]. Hydrometallurgy, which offers the advantages of lower capital cost and higher selectivity than pyrometallurgy, is an alternative approach [12]. In this process, E-waste is digested by a suitable leaching agent, such as aqua regia, and the precious metals can be selectively captured and recovered from the leach liquor, for example by electrowinning, chemical reduction, or adsorption. Obviously, a low cost method involving adsorption with minimal environmental impact would be ideal for recovering precious metals from the acid-digested solution [13–15]. However, traditional adsorbents such as activated carbons and mesoporous oxides are poorly adsorbant and poorly selective for the precious metal ions at low concentrations in the leach liquor. Therefore, it is of great interest and importance to develop advanced adsorbents that are highly adsorbant and selective, reliably stable and easily recyclable, with fast kinetics, for efficiently recovering precious metals from E-waste.

Porous organic materials (POMs) are a new family of functional nanoporous materials constructed by linking pure organic monomers via strong covalent bonds [16–19]. They usually possess a high surface area (up to 7,000 m^2/g) and tuneable pore sizes, and have demonstrated great potential in gas storage and separation [20,21], air and water purification [22–24], energy storage [25], and catalysis [26,27]. More importantly, their synthetic diversity allows for precise control over their structure and functionality through the judicious selection of building blocks and connection nodes. Therefore, POMs with tunable

* Corresponding author at: Division of Nanotechnology and Functional Materials, Department of Materials Science and Engineering, Ångström Laboratory, Uppsala University, Uppsala SE-75121, Sweden.
E-mail address: chao.xu@angstrom.uu.se (C. Xu).

https://doi.org/10.1016/j.cej.2023.141498
Received 3 November 2022; Received in revised form 26 December 2022; Accepted 16 January 2023
Available online 18 January 2023

compositions and porous structures, along with rich surface functionalities, can potentially fulfil the requirements for efficient adsorbents of precious metals from E-waste [13,14,28–33]. For example, Stoddart and Yavuz developed a family of porous polymers consisting of porphyrin units for efficiently recovering gold and platinum from E-waste via the reductive activity of the porphyrin units and their strong interactions with the precious metals [34]. We have recently reported the synthesis of an ionic covalent organic framework (COF) for palladium scavenging. The ionic framework and porous structure of this COF allow it to efficiently scavenge trace amounts of $[PdCl_4]^{2-}$ in aqueous solution, with high adsorption capacities of up to 754 mg/g of COF, via a chemisorption (ion exchange) process [35]. To date, the practical application of POMs in precious metal recovery has rarely been exploited, probably because of the difficulties associated with shaping and processing the insoluble POM powders and the high costs of synthesis.

Fortunately, modern materials science and nanotechnology now offer opportunities for overcoming the drawback of difficulties in processing POMs. From a materials science point of view, cellulose has several advantages, such as its hierarchical porosity and fibrous nanostructure, high surface area, excellent flexibility, and rich organic functionalities, which make it an ideal substrate and template for the nanofabrication of various bulk materials [36,37]. Recently, we have developed nanocompositing techniques for fabricating porous materials (e.g., metal–organic frameworks, COFs, porous carbons), with the assistance of cellulose, into freestanding nanopapers and aerogels which have hierarchical porosity, high mechanical strength, and excellent flexibility [38–45]. The nanopapers can be used as efficient filters for cleaning air, or electrodes for assembling flexible devices for energy storage and harvesting. Herein, we report a facile interweaving technique for processing an ionic COF material into freestanding nanopapers with the assistance of commercial filter paper-based cellulose fibers (CF). We also investigated the adsorption kinetics, adsorption capacity and selectivity of both the COP and CF-COF nanopapers for trace amounts of $[AuCl_4]^-$ in aqueous solution. In addition, we investigated the efficacy of the CF-COF nanopapers to withstand continuous, long-term capture of gold species from flowing E-waste leaching solutions.

2. Results and discussion

In a typical hydrometallurgy process, E-waste is digested in aqua regia to dissolve metals. Common metal elements such as Cu, Zn, Sn, Fe, Pb, Al and Ni are dissolved into metal cations, while Au is converted into $[AuCl_4]^-$ anions. The theory is that the ionic COF materials with cationic frameworks and anionic counter-ions could selectively capture $[AuCl_4]^-$ anions from the metal leachate due to the ion exchange mechanism. The cationic COF network could have strong electrostatic interaction with $[AuCl_4]^-$ anions while repulsing other metal cations [46]. The addition of specific functional groups such amines to the COFs could reduce $[AuCl_4]^-$ anions to Au^0 as a result of the high reduction potential of $[AuCl_4]^-$ and the reductive activity of the amines. Therefore, the synergetic effects of physisorption, ion exchange and chemical reduction of $[AuCl_4]^-$ on the ionic COF materials could result in significantly higher capture capacity and selectivity than a conventional physisorption process. In this context, we synthesized a guanidinium-based ionic COF for studying gold recovery from E-waste. The $TpTG_{Cl}$ COF was synthesized by condensation of 1,3,5-triformylphloroglucinol (Tp) and triaminoguanidiniumchloride (TG_{Cl}) in a hydrothermal reaction (Fig. 1a)

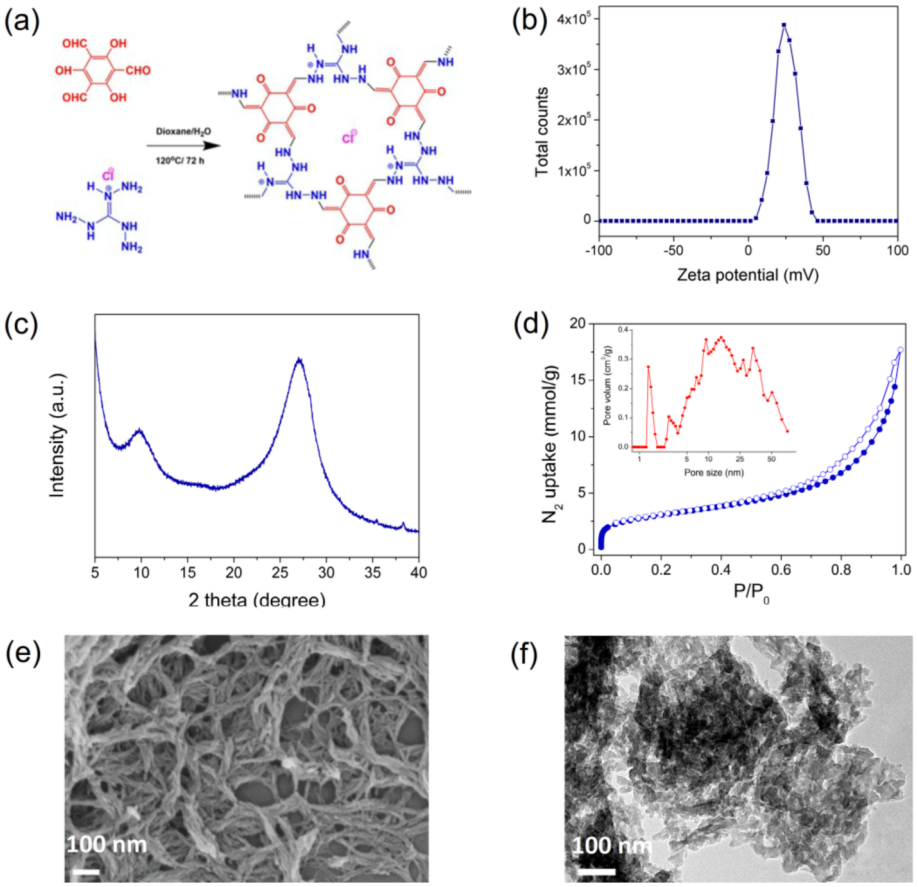

Fig. 1. (a) Synthesis of $TpTG_{Cl}$ COF; (b) zeta potential of an aqueous suspension of $TpTG_{Cl}$ COF; (c) powder X-ray diffraction pattern for $TpTG_{Cl}$ COF; (d) N_2 adsorption and desorption isotherms for $TpTG_{Cl}$ COF recorded at 77 K. The inset shows the pore size distribution of $TpTG_{Cl}$ COF calculated from the adsorption isotherm using density functional theory model. (e) Scanning electron microscopy and (f) transmission electron microscopy images of $TpTG_{Cl}$ COF.

[35,47,48]. The aqueous suspension of fine particles of $TpTG_{Cl}$ COF (~0.4 mg/mL) exhibited a positive zeta potential of + 25.7 mV, indicating the cationic structure of the COF (Fig. 1b). The presence of chloride counter ions was revealed by strong peaks for Cl $2p_{1/2}$ and Cl $2p_{3/2}$ at 197.71 and 199.38 eV, respectively, under X-ray photoelectron spectroscopy (XPS; Fig. S1). Energy-dispersive X-ray spectroscopy (EDS) elemental mapping also confirmed the presence of Cl in $TpTG_{Cl}$ COF (Fig. S2). The molecular structure was studied using infrared (IR) and solid-state ^{13}C nuclear magnetic resonance (NMR) spectroscopy (Fig. S3 and S4). The strong double peaks at 1593 and 1621 cm^{-1} in the IR spectrum were assigned to the C═C and C═O stretching vibrations, respectively. The infrared peak band at 1288 cm^{-1} was attributed to the C — N stretching vibration. The NMR signals for the chemical shifts at 99.7 and 161.5 ppm were assigned to the carbon atoms of C═C and C═O, respectively, located on the C6 member rings. The signal for the carbon atoms in C — N linkages was found at 149.9 ppm.

More detailed assignments and analyses of the IR and NMR spectra are provided in the Supporting Information (Fig. S3 and S4). The spectroscopic studies indicated that the framework consisted of a keto-enamine structure which was formed by reversible Schiff-base condensation and irreversible enol to keto tautomerization. The keto-enamine linkages endowed $TpTG_{Cl}$ COF with high physiochemical stability that the structure of $TpTG_{Cl}$ COF had no significant change after soaking the sample in in an aqueous HCl solution (pH = 2.0) for 24 h (Fig. S5). The powder X-ray diffraction (XRD) pattern for the $TpTG_{Cl}$ COF displayed broad peaks at 9.8° and 27.5°, corresponding to (100) and (001) planes, respectively (Fig. 1c). The weak crystallinity may be the result of an ionic feature, namely that repulsion of the cationic layers hampered the formation of a highly ordered and stacked structure. $TpTG_{Cl}$ COF had a relatively high Brunauer, Emmett, Teller (BET) surface area of 247.7 m^2/g. Analysis of the adsorption isotherm revealed the presence of both micropores and mesopores with pore sizes centered at 1.5 and 18 nm, respectively (Fig. 1d). Interestingly, $TpTG_{Cl}$ COF was nanofibrous in structure, with a fiber thickness of ~ 50 nm, as shown in the scanning electron microscopy (SEM) image; this differed from the morphology of the same nanosheets reported in previous studies (Fig. 1e) [47,49]. High-resolution transmission electron microscopy (TEM) images clearly showed the irregular mesopores between the nanofibers (Fig. 1f). Therefore, the micropores were generated from the polymer network, while the mesopores were generated from aggregation of the nanofibers. It is noteworthy that the stacked nanofibrous structure not only formed the mesopores that could increase mass transport during the adsorption process, but may also have facilitated dispersion of the material in water, which would be greatly beneficial for material processing.

Because of its relatively high surface area, hierarchical porosity, ionic structure and rich amine content, $TpTG_{Cl}$ COF was used to capture $[AuCl_4]^-$ from aqueous solution. Both adsorption kinetics and capacity were studied in detail. Specifically, $TpTG_{Cl}$ COF powder was mixed with de-ionized water. The mixture was then easily sonicated into a homogeneous brown suspension because of its ionic framework and the associated high hydrophilicity. A clear Tyndall effect was observed with the suspension (Fig. S6). Once the suspension was mixed with an aqueous solution of $Na[AuCl_4]\bullet 2H_2O$ (100 ppm of Au; pH = ~3.0), it turned dark brown and then immediately became black (Fig. 2a). The obvious color change was probably the result of reduction of $[AuCl_4]^-$ to form gold nanoparticles. The adsorption capacity reached 1,794 mg Au/

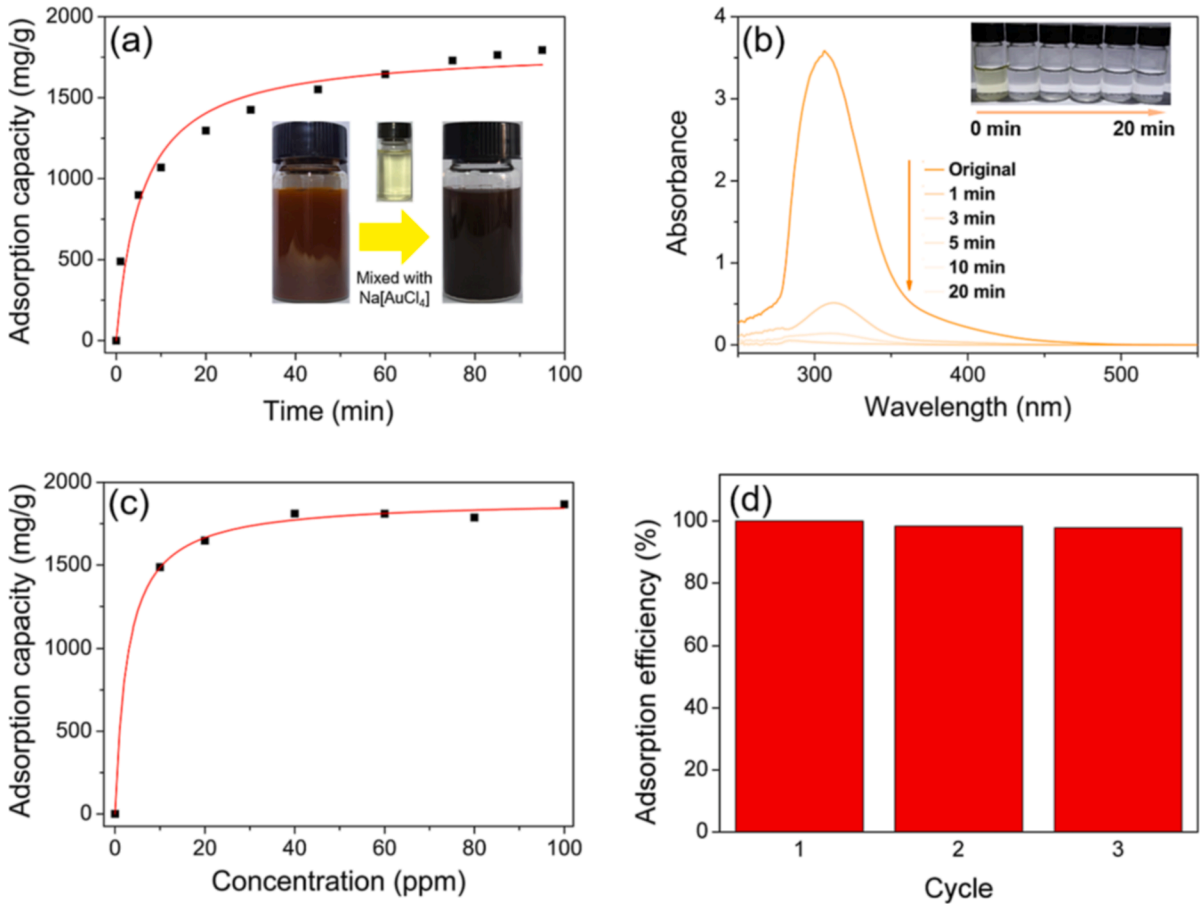

Fig. 2. $TpTG_{Cl}$ COF for recovering trace amounts of $[AuCl_4]^-$ in aqueous solution. (a) Kinetic curve of $Na[AuCl_4]\bullet 2H_2O$ capture on $TpTG_{Cl}$ COF. The inset shows the color change of the aqueous suspension of $TpTG_{Cl}$ COF upon mixing with $Na[AuCl_4]\bullet 2H_2O$ solution; (b) UV–vis spectra of aqueous $Na[AuCl_4]\bullet 2H_2O$ solutions at different intervals during the scavenging experiment. The inset compares optical images of aqueous $Na[AuCl_4]\bullet 2H_2O$ solution and the solution after the scavenging experiment; (c) $Na[AuCl_4]\bullet 2H_2O$ adsorption isotherm of $TpTG_{Cl}$ COF; (d) $Na[AuCl_4]\bullet 2H_2O$ capture performance on $TpTG_{Cl}$ COF for three consecutive cycles.

g of $TpTG_{Cl}$ COF at 95 min. More importantly, the kinetic study indicated fast capture of $[AuCl_4]^-$ by $TpTG_{Cl}$ COF in that the capacity reached 27.3 % and 59.6 % of the saturation capacity in 1 and 10 min, respectively. The kinetic curve fitted well with a pseudo–second-order kinetic model giving a correlation coefficient value of 0.968, which was much higher than that of the analysis using a pseudo-first-order kinetic model (0.919) (Fig. 2a and S7). This suggests that the capture process was dominated by chemical adsorption associated with electron transfer between $TpTG_{Cl}$ COF and $[AuCl_4]^-$. The main rate-limiting step is chemical adsorption rather than interparticle diffusion [50]. In addition, $[AuCl_4]^-$ can be fully removed from the solution by increasing the amount of $TpTG_{Cl}$ COF. As shown in Fig. 2b, the aqueous solution of $[AuCl_4]^-$ (227.5 mL, 213 ppm of Au) changed from yellow to colorless in a few minutes after mixing with 90 mg of $TpTG_{Cl}$ COF. The time-dependent UV–vis spectra recorded during the capture process revealed the rapid removal of $[AuCl_4]^-$ from the solution. Remarkably, the capacity maintained a high value (1,478 mg Au/g of $TpTG_{Cl}$ COF) at an ultra-low concentration of 10 ppm of $[AuCl_4]^-$. The adsorption isotherm agreed well with Langmuir adsorption, giving a high maximum adsorption capacity of 1,895 mg Au/g of $TpTG_{Cl}$ COF (Fig. 2c and S8). More importantly, the COF performed well in capturing gold for at least three consecutive adsorption/desorption cycles (Fig. 2d). It is worthy to note that $TpTG_{Cl}$ COF had lower adsorption capacities of Au in neutral and basic solutions (Fig. S9), which can be attribute to the weaker electrostatic interactions between $[AuCl_4]^-$ and the $TpTG_{Cl}$ COF with lower zeta potentials at higher pH values (Fig. S10).

The solid deposit from the mixture was collected by centrifugation once the capture process reached equilibrium. The composition and structure of the collected solid ($TpTG_{Cl}$ COF-Au) was investigated to reveal the mechanism of the gold capture process. The IR spectra of the sorbent did not change significantly upon capturing $[AuCl_4]^-$, which indicated the high chemical stability of $TpTG_{Cl}$ COF (Fig. S11). $TpTG_{Cl}$ COF-Au displayed sharp diffraction peaks for elemental Au as observed in the XRD pattern, which indicated the reduction of $[AuCl_4]^-$ during the capture process (Fig. 3a). Since the capture of $[AuCl_4]^-$ and the formation of elemental Au on $TpTG_{Cl}$ COF increased the bulk density and blocked the pores, the surface area and total pore volume were significantly reduced from 247.7 m^2/g and 0.476 cm^3/g for $TpTG_{Cl}$ COF to 84.8 m^2/g and 0.156 cm^3/g for $TpTG_{Cl}$ COF-Au (Fig. 3b). The thermogravimetric analysis (TGA) curve of $TpTG_{Cl}$ COF-Au in the temperature range 25–800 °C was recorded under air atmosphere and the composition of the residue was determined to be pure elemental Au, based on the XRD study (Fig. S12). The large amount of the residue was consistent with the high capture capacities of COF for $[AuCl_4]^-$. The SEM image of $TpTG_{Cl}$ COF-Au showed deposition of nanoparticles sized ~ 100 nm on the surface of the $TpTG_{Cl}$ COF substrate (Fig. 3c). The TEM images clearly and consistently showed that the nanoparticles were evenly distributed on the substrate, with sharp contrast between the nanoparticles and the substrate (Fig. 3d). Further studies coupled with EDS and elemental mapping confirmed that the nanoparticles were made of elemental Au (Fig. 3e).

In addition, a set of *ex-situ* studies using zeta potential readings, SEM and XPS were carried out to monitor the process of capturing $[AuCl_4]^-$ on $TpTG_{Cl}$ COF to improve our understanding of the detailed mechanism of the $[AuCl_4]^-$ adsorption process. Firstly, a series of mixtures were prepared by adding different amounts of $Na[AuCl_4]\bullet 2H_2O$ into an aqueous suspension of $TpTG_{Cl}$ COF to give a mass ratio of $Na[AuCl_4]\bullet 2H_2O/TpTG_{Cl}$ COF ranging from 1:50 to 4:1. The zeta potential was measured after the mixtures had been stirred for 1 h. Interestingly, the zeta potential gradually decreased from + 15.8 mV for pure $TpTG_{Cl}$ COF to − 35.7 mV with increasing amounts of $Na[AuCl_4]\bullet 2H_2O$. The decreased zeta potential may be explained by the formation of gold nanoparticles with a negatively charged surface and subsequent deposition of the nanoparticles on the COF substrate. SEM images of the collected solids showed that the visible density of the gold nanoparticles on the substrate significantly increased with increasing $Na[AuCl_4]\bullet$

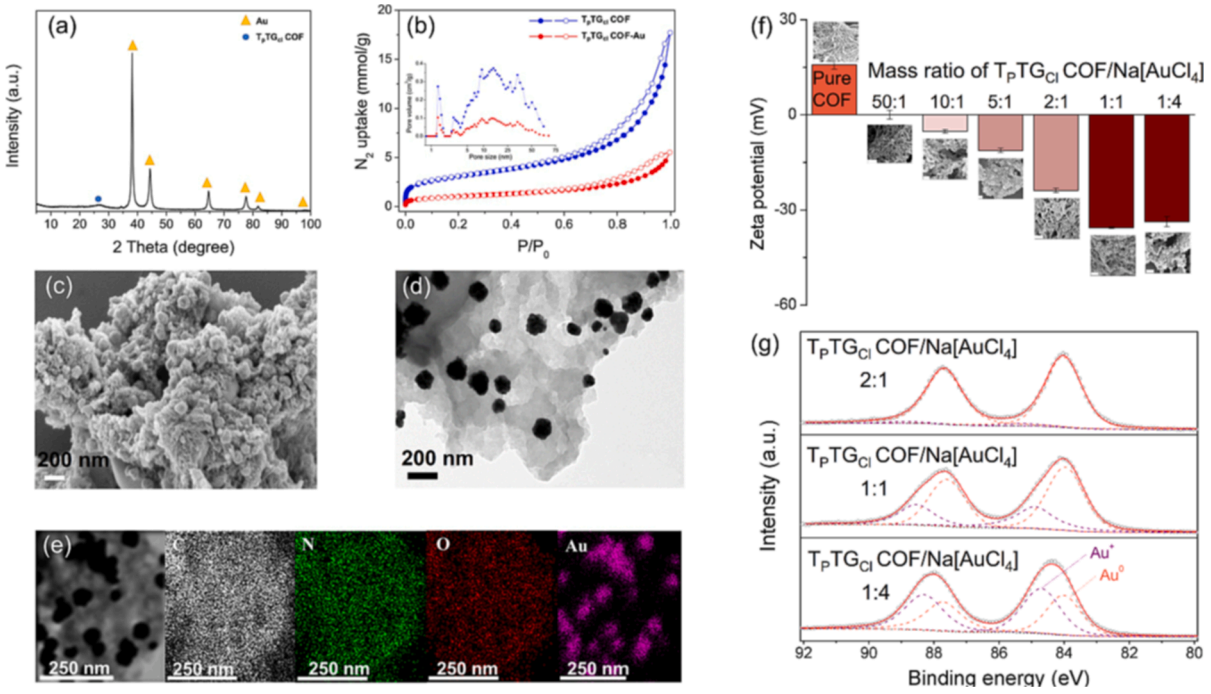

Fig. 3. (a) Powder X-ray diffraction pattern of the collected solid deposit of $TpTG_{Cl}$ COF-Au after gold capture. A mass ratio of $TpTG_{Cl}$ COF:$Na[AuCl_4]$ of 1:4 was used for the gold capture experiment. (b) Comparison of N_2 sorption isotherms (77 K) for $TpTG_{Cl}$ COF-Au and $TpTG_{Cl}$ COF. The inset compares the pore size distributions for $TpTG_{Cl}$ COF-Au and $TpTG_{Cl}$ COF. (c) Scanning electron microscopy and (d) transmission electron microscopy images of $TpTG_{Cl}$ COF-Au. (e) Elemental mapping for $TpTG_{Cl}$ COF-Au. (f) The chart compares the variations in the zeta potential of $TpTG_{Cl}$ COF aqueous suspension upon mixing with different amounts of $Na[AuCl_4]\bullet 2H_2O$. The insets are SEM images of the collected solid deposits from the suspensions containing $TpTG_{Cl}$ COF/$Na[AuCl_4]$ with different mass ratios (enlarged SEM images are shown in Fig. S13). (g) High-resolution Au 4f X-ray photoelectron spectra with deconvoluted results for the collected solids.

$2H_2O$ concentrations (Fig. 3f and S13). In addition, the collected solids were characterized by XPS to analyse the oxidation state of the gold species enriched on the COF. The high resolution Au 4f spectrum of the collected sample from the mixture with a $Na[AuCl_4]\bullet 2H_2O$/TpTGCl COF ratio of 1:2 indicated the formation of mainly elemental Au^0 with a binding energy of 83.99 eV. In comparison, the binding energy for the gold species shifted positively by 0.12 and 0.36 eV upon increasing the ratio to 1:1 and 4:1, respectively. The Au 4f XPS spectra for the latter two samples were deconvoluted into two peaks at 84.9 and 83.9 eV, corresponding to Au^+ and Au^0, respectively [34]. The Au^+ was probably present in the reduced form of the $[AuCl_2]^-$ species, which can be adsorbed onto $TpTG_{Cl}$ COF via ion exchange and/or electrostatic interactions. In addition, increasing the ratio resulted in an increase of the percentage of Au^+ in the sample. However, no significant signal for Au^{3+} was found in the XPS spectra (Fig. 3g). The reduction potential of the $TpTG_{Cl}$ COF (−1.16 V) was more negative than the redox potential of $[AuCl_4]^-$ to Au^0 (1.002 V vs a normal hydrogen electrode [NHE]) and $[AuCl_4]^-$ to $[AuCl_2]^-$ (0.926 V vs an NHE), which makes the reduction process thermodynamically allowed (Fig. S14) [29,51]. The reduction was most probably driven by the rich amine species in $TpTG_{Cl}$ COF that served as the reducing agent. These findings suggested that $[AuCl_4]^-$ species at low loading amounts can be fully reduced to Au^0 nanoparticles by the $TpTG_{Cl}$ COF adsorbent, while a higher loading amount of $[AuCl_4]^-$ resulted in the formation of both $[AuCl_2]^-$ species and Au^0 nanoparticles due to the limited reduction capacity of the adsorbent (Scheme S1).

In contrast to the process of $[AuCl_4]^-$ capture, the kinetics of the adsorption of Cu^{2+} onto $TpTG_{Cl}$ COF was much slower, and the capacity was lower: up to 55.3 mg Cu/g $TpTG_{Cl}$ COF at 100 ppm (Fig. S15). The low adsorption capacity can be explained by the repulsive effect between the cationic COF framework and Cu^{2+}. In addition, there were no diffraction peaks of elemental Cu in the XRD pattern of the collected COF sample after adsorption (Fig. S16). Consistently, the high resolution of the Cu 2p XPS spectrum only displayed peaks for Cu^{2+} (Fig. S17). These results suggest that the adsorption of Cu^{2+} onto $TpTG_{Cl}$ COF is a purely physical process. Therefore, $TpTG_{Cl}$ COF is expected to selectively capture $[AuCl_4]^-$ from a solution containing mixed metal ions.

From a practical application point of view, the use of $TpTG_{Cl}$ COF powder for capturing gold from E-waste is not feasible because separation of the fine gold-enriched COF particles from the highly diluted solution is complicated and energy intensive. It thus would be greatly beneficial to develop membranes based on $TpTG_{Cl}$ COF that would allow the use of a membrane separation technique for capturing gold. Gold species can be captured and enriched on the membrane used as a fixed filter by continuously flowing the solution through the membrane. We therefore fabricated freestanding nanopapers consisting of $TpTG_{Cl}$ COF and cellulose fibers, using an interweaving technique. Specifically, a well-dispersed suspension of $TpTG_{Cl}$ COF in water was thoroughly mixed with an aqueous suspension of commercial filter nanopaper-based cellulose fibers using probe sonication. Flexible, foldable, free-standing CF-COF nanopapers were prepared by filtering the mixture through a polyethersulfone membrane (pore diameter: 0.45 μm), followed by drying and peeling off procedures (Fig. 4a). This nano-engineering approach took advantage of the good processability and nano/microfibrous structure of cellulose fibers and the good water-dispersibility of $TpTG_{Cl}$ COF. In addition, the natural abundance, biodegradability and low cost of cellulose and the use of water as the only solvent provided environmental advantages. The XRD patterns for the CF-COF nanopaper displayed weak diffraction peaks for $TpTG_{Cl}$ COF at 2θ of 9.8° and 27.5° and intensive peaks for cellulose at 2θ of 15.0°, 16.8°, 22.9° and 34.5° (Fig. 4b). Comparison of the XRD patterns for the $TpTG_{Cl}$ COF, CF, and CF-COF nanopapers suggested that both $TpTG_{Cl}$ COF and CF maintained their crystalline structure during the nano-engineering process (Fig. S18a). In addition, the hierarchical porosity of $TpTG_{Cl}$ COF remained in the CF-COF nanopaper, resulting in a surface area of 100.3 m^2/g and the presence of pores with pore sizes centered at 1.5 and 30 nm (Fig. 4c). The $TpTG_{Cl}$ COF content in the nanopaper was calculated as ~ 52 wt% by analysing the TGA curves for the CF-COF nanopaper, $TpTG_{Cl}$ COF and CF (Fig. S19). The top view SEM images for the CF-COF nanopaper clearly showed that the COF particles were interwoven through the cellulose micro- and nanofibers and were evenly dispersed within the network (Fig. 4d-e and S20). The side view of the nanopaper showed a similar mixed matrix structure (Fig. 4f-g). Given the compact and interconnected nanostructure, the nanopaper displayed relatively high mechanical strength with tensile strength of 1.84 MPa and Young's modulus of 71.98 MPa, respectively (Fig. S21).

Obviously, the freestanding, flexible features of CF-COF nanopapers with high water flux (~158.7 $L/m^2/h$) enabled their use for membrane separation. Firstly, the removal performances of the CF-COF nanopapers for $[AuCl_4]^-$ and Cu^{2+} from the aqueous solutions were evaluated. Specifically, an aqueous solution of $Na[AuCl_4]\bullet 2H_2O$ (505 mL, 50 ppm of Au) was flowed through a CF-COF nanopaper (effective area: 3.8 cm^2, $TpTG_{Cl}$ COF loading density: 3.55 mg/cm^2) at a constant flow rate of 1.0 mL/min. The concentration of $Na[AuCl_4]\bullet 2H_2O$ in the outlet solution was measured at various intervals. Remarkably, the concentration of Au remained at low values of < 1 ppm for up to 200 min, indicating that the CF-COF nanopaper had a high removal efficiency for the initial 200 mL of solution. The concentration then gradually increased to 10.86 ppm at 320 min and finally reached 43.52 ppm at the end of the experiment, indicating that the nanopaper displayed overall removal rates of 99 % and 74.3 % for the initial 200 mL solution and the total solution, respectively (Fig. 5a-b). When increasing the flow rate to 2.0 mL/min, the CF-COF nanopaper displayed a slightly lower removal efficiency that the overall removal rate was 87.2 % for the initial 200 mL solution

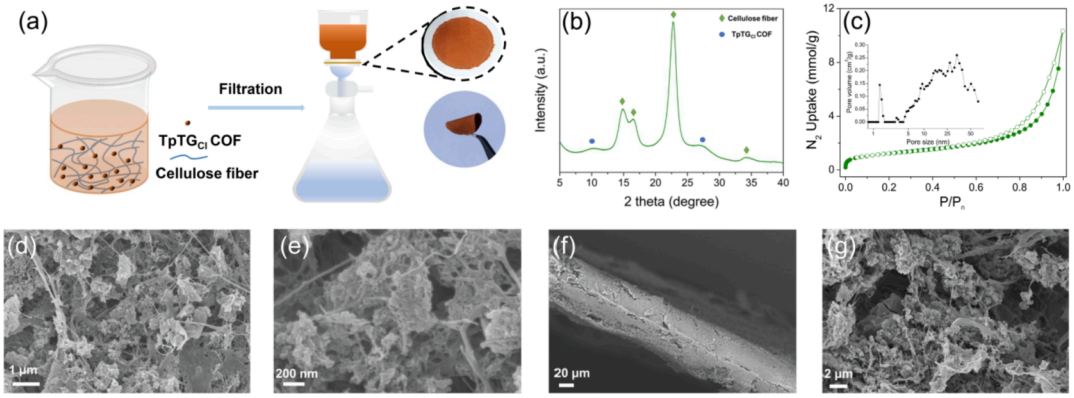

Fig. 4. (a) Schematic illustration of the preparation of freestanding CF-COF nanopaper from cellulose fibers and $TpTG_{Cl}$ COF; (b) powder X-ray diffraction pattern of CF-COF nanopaper; (c) N_2 sorption isotherm and pore size distribution of CF-COF nanopaper. Scanning electron microscopy images of CF-COF nanopaper from (d-e) top view and (f-g) side view, at different magnifications.

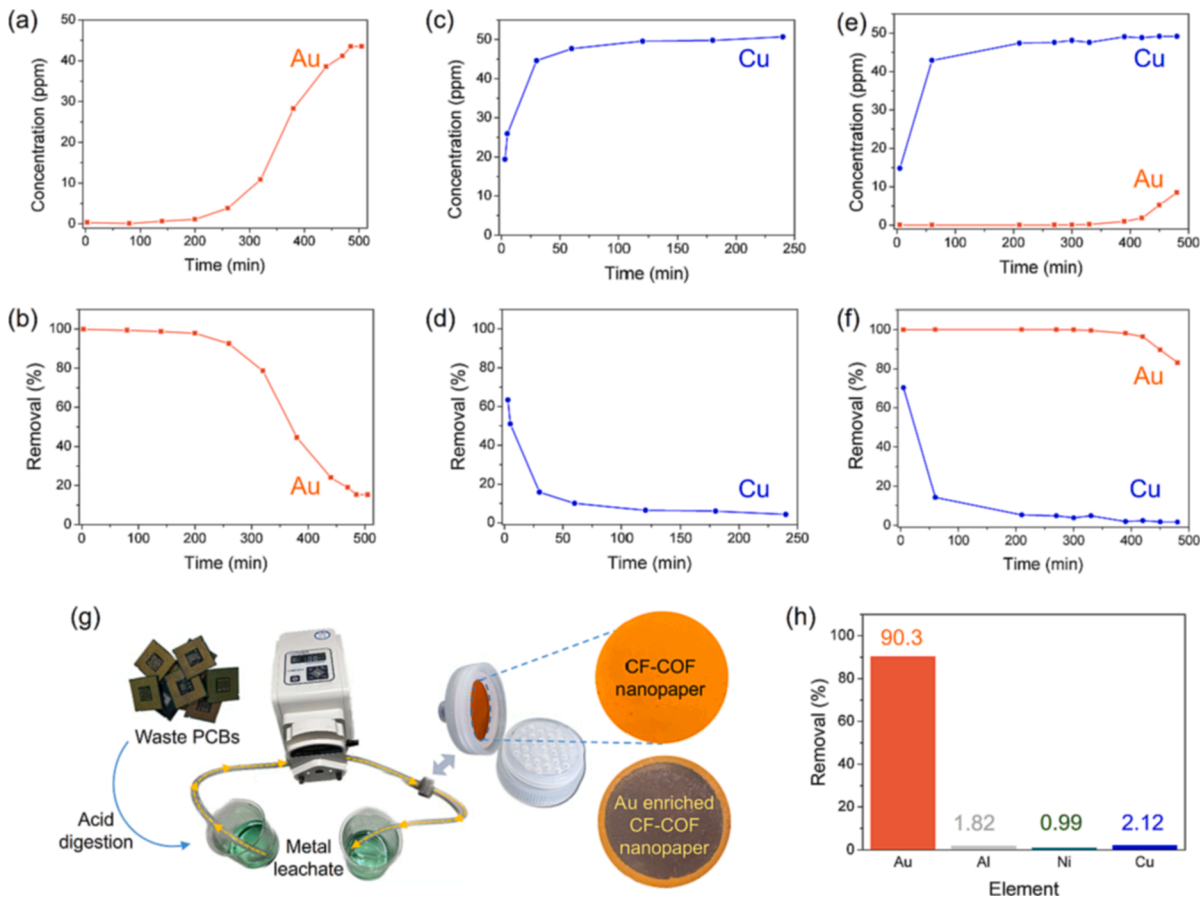

Fig. 5. Membrane separation performances of CF-COF nanopapers in an aqueous solution of (a-b) $Na[AuCl_4]\bullet 2H_2O$ (50 ppm of Au); (c-d) $Cu(NO_3)_2{\cdot}3H_2O$ (50 ppm of Cu); and (e-f) a mixed solution consisting of both $Na[AuCl_4]\bullet 2H_2O$ (50 ppm of Au) and $Cu(NO_3)_2{\cdot}3H_2O$ (50 ppm of Cu). (g) Schematic illustration of the whole process of gold capture from printed circuit board (PCB) waste based on CF-COF nanopapers. (h) Capture efficiencies of different metals from the PCBs.

(Fig. S22). The slightly decreased efficiency can be explained by the reduced interaction time between the CF-COF nanopaper and the solute during the separation. More importantly, the CF-COF film demonstrated relatively good cyclic performance for capturing Au from the aqueous solution (Fig. S23). In contrast, removal rates with the CF-COF nanopaper for the $Cu(NO_3)_2{\cdot}3H_2O$ solution were significantly lower under the same conditions (flow rate: 1 mL/min). The removal rate was only 63.3 % in the initial stage of the experiment and it decreased rapidly to 15.75 % at 30 min and to < 10 % after 60 min. The overall removal rate was calculated to be as low as 10.5 % (Fig. 5c–d). In addition, the removal performance of the CF-COF nanopaper was evaluated for a solution containing both $Na[AuCl_4]\bullet H_2O$ (50 ppm) and $Cu(NO_3)_2{\cdot}3H_2O$ (50 ppm) (Fig. 5e–f). Remarkably, the presence of Cu^{2+} in the solution had no influence on the capture of $[AuCl_4]^-$. The nanopaper (effective area: 3.8 cm^2, $TpTG_{Cl}$ COF loading density: 3.7 mg/cm^2) showed extremely high removal rates of 99.9 % and 96.4 % for $[AuCl_4]^-$ at 300 and 420 min, respectively, in contrast to negligible removal rates of 3.8 % and 2.4 % for Cu^{2+} at the same intervals. These results were fully consistent with the adsorption studies in that both $TpTG_{Cl}$ COF and CF-COF nanopapers displayed a high capacity and selectivity for trace amounts of $Na[AuCl_4]\bullet H_2O$ from aqueous solution. Thereafter, in a proof-of-concept study, we used the CF-COF nanopapers as membranes for capturing gold species from the E-waste leaching solution, which was prepared by digestion of printed circuit board (PCB) waste in aqua regia (Fig. 5g). The pH value of the mixture was adjusted to ~2.0 and any undissolved solids in the mixture were removed by centrifugation. Inductively coupled plasma atomic emission spectroscopy (ICP-AES) analysis indicated that the obtained solution contained significant amounts of Cu (3780.8 ppm) and Ni (512.55 ppm) and trace amounts of Al (13.51 ppm) and Au (8.92 ppm). The removal rate for the CF-COF nanopaper was > 90 % for Au, which was much higher than the values for the other elements (Fig. 5h). Due to the selective reduction of gold species by the $TpTG_{Cl}$ COF component in the CF-COF nanopaper, the collected nanopaper displayed characteristic diffraction peaks for elemental Au, while no diffraction peaks of other metals were observed (Fig. S24). In contrast to the use of sorbent powders to capture gold, which required an additional separation procedure to isolate the sorbents (Fig. S25-26, Table S1), the gold-enriched CF-COF nanopapers can be directly subjected to refining processes to obtain gold with high purity. In addition, the membrane separation process was more time-efficient than reported studies based on conventional adsorption techniques [13,14,28–35].

Finally, we calculated the economics of gold recovery from E-waste using the CF-COF nanopapers. Based on the cost of the chemical starting materials, $TpTG_{Cl}$ COF can be synthesized in the lab at a cost of ~ $0.97/g (Table S2) and the preparation of 10 pieces of CF-COF membrane (diameter: 5 cm, thickness: 0.2 mm, weight: 200 mg, mass loading of COF: ~50 wt%) cost ~$2. Since 1 g of the COF can capture 1.794 g of gold, the gold captured by 10 pieces of CF-COF membranes would be worth $103.5 (calculated based on the current gold price, $57.7/g). The profit margin could be further increased by large-scale production of the membranes.

3. Conclusion

A facile and environmentally friendly nanoengineering technique has been developed for processing COF materials into freestanding, flexible nanopapers with the assistance of commercial filter paper-based

cellulose fibers. The COF particles were interwoven with the cellulose fibers to form a compact, homogeneous network in the nanopapers. The ionic structure and the nanofibrous structure of the COF, along with the excellent processability of the cellulose fibers, played a key role in the success of the process. The nanopapers had extremely high capture capacity, and good kinetics and selectivity for trace amounts of $[AuCl_4]^-$ in the aqueous solution as a result of the synergetic effects of physical adsorption, ion exchange and chemical reduction of the gold species on the COF. A proof-of-concept study demonstrated that the nanopaper-based membranes could capture gold species from metal leachates of PCB waste with high efficiency and good selectivity. Further studies could focus on growing COF nanolayers on the surface of cellulose nanofibers via an interfacial synthetic method. The precious metal recovery performance of nanopapers composed of such integrated nanofibers would be expected to be superior. It is hoped that this study promotes the development of freestanding sustainable membranes based on porous organic materials and their application in various separation processes related to E-waste recycling.

CRediT authorship contribution statement

Qinqin Xu: Methodology, Investigation. **Xing-Hao Du:** Methodology, Investigation. **Dan Luo:** Methodology, Investigation. **Maria Strømme:** Writing – review & editing. **Qian-Feng Zhang:** Writing – review & editing. **Chao Xu:** Conceptualization, Methodology, Investigation, Supervision, Writing – original draft, Writing – review & editing.

Declaration of Competing Interest

The authors declare that they have no known competing financial interests or personal relationships that could have appeared to influence the work reported in this paper.

Data availability

Data will be made available on request.

Acknowledgement

This project was supported by the Åforsk grant, the Natural Science Foundation of China (90922008) and the Anhui Provincial Natural Science Foundation (2108085QB72). We wish to thank Prof. Martin Sjödin for valuable discussions concerning the electrochemical experiments.

Appendix A. Supplementary data

Supplementary data to this article can be found online at https://doi.org/10.1016/j.cej.2023.141498.

References

[1] R. Rautela, S. Arya, S. Vishwakarma, J. Lee, K.-H. Kim, S. Kumar, E-waste management and its effects on the environment and human health, Sci. Total Environ. 773 (2021), 145623, https://doi.org/10.1016/j.scitotenv.2021.145623.
[2] A.K. Awasthi, J. Li, L. Koh, O.A. Ogunseitan, Circular economy and electronic waste, Nat. Electron. 2 (3) (2019) 86–89, https://doi.org/10.1038/s41928-019-0225-2.
[3] R. Nithya, C. Sivasankari, A. Thirunavukkarasu, Electronic waste generation, regulation and metal recovery: a review, Environ. Chem. Lett. 19 (2) (2021) 1347–1368, https://doi.org/10.1007/s10311-020-01111-9.
[4] K. Zhang, J.L. Schnoor, E.Y. Zeng, E-Waste Recycling: Where Does It Go from Here? Environ. Sci. Technol. 46 (20) (2012) 10861–10867, https://doi.org/10.1021/es303166s.
[5] C.B. Tabelin, I. Park, T. Phengsaart, S. Jeon, M. Villacorte-Tabelin, D. Alonzo, K. Yoo, M. Ito, N. Hiroyoshi, Copper and critical metals production from porphyry ores and E-wastes: A review of resource availability, processing/recycling challenges, socio-environmental aspects, and sustainability issues, Resour. Conserv. Recycl. 170 (2021), 105610, https://doi.org/10.1016/j.resconrec.2021.105610.
[6] V. Forti, C. Peter Baldé, R. Kuehr, G. Bel, The Global E-waste Monitor 2020, The Global E-waste Monitor 2020 (2020).
[7] X. Zeng, J.A. Mathews, J. Li, Urban Mining of E-Waste is Becoming More Cost-Effective than Virgin Mining, Environ. Sci. Technol. 52 (8) (2018) 4835–4841, https://doi.org/10.1021/acs.est.7b04909.
[8] E.R. Rene, M. Sethurajan, V. Kumar Ponnusamy, G. Kumar, T.N. Bao Dung, K. Brindhadevi, A. Pugazhendhi, Electronic waste generation, recycling and resource recovery: Technological perspectives and trends, J. Hazard. Mater. 416 (2021), 125664, https://doi.org/10.1016/j.jhazmat.2021.125664.
[9] M.D. Rao, K.K. Singh, C.A. Morrison, J.B. Love, Challenges and opportunities in the recovery of gold from electronic waste, RSC Adv. 10 (8) (2020) 4300–4309, https://doi.org/10.1039/C9RA07607G.
[10] B. Deng, D.X. Luong, Z. Wang, C. Kittrell, E.A. McHugh, J.M. Tour, Urban mining by flash Joule heating, Nat. Commun. 12 (1) (2021) 5794, https://doi.org/10.1038/s41467-021-26038-9.
[11] H. Wang, S. Zhang, B. Li, De'an Pan, Y. Wu, T. Zuo, Recovery of waste printed circuit boards through pyrometallurgical processing: A review, Resour. Conserv. Recycl. 126 (2017) 209–218, https://doi.org/10.1016/j.resconrec.2017.08.001.
[12] M. Sethurajan, E.D. van Hullebusch, D. Fontana, A. Akcil, H. Deveci, B. Batinic, J. P. Leal, T.A. Gasche, M. Ali Kucuker, K. Kuchta, I.F.F. Neto, H.M.V.M. Soares, A. Chmielarz, Recent advances on hydrometallurgical recovery of critical and precious elements from end of life electronic wastes - a review, Crit. Rev. Environ. Sci. Technol. 49 (3) (2019) 212–275, https://doi.org/10.1080/10643389.2018.1540760.
[13] D.T. Sun, N. Gasilova, S. Yang, E. Oveisi, W.L. Queen, Rapid, Selective Extraction of Trace Amounts of Gold from Complex Water Mixtures with a Metal-Organic Framework (MOF)/Polymer Composite, J. Am. Chem. Soc. 140 (48) (2018) 16697–16703, https://doi.org/10.1021/jacs.8b09555.
[14] R. Ding, Y. Chen, Y. Li, Y. Zhu, C. Song, X. Zhang, Highly Efficient and Selective Gold Recovery Based on Hypercross-Linking and Polyamine-Functionalized Porous Organic Polymers, ACS Appl. Mater. Interfaces 14 (9) (2022) 11803–11812, https://doi.org/10.1021/acsami.1c22514.
[15] T.S. Nguyen, Y. Hong, N.A. Dogan, C.T. Yavuz, Gold Recovery from E-Waste by Porous Porphyrin-Phenazine Network Polymers, Chem. Mater. 32 (12) (2020) 5343–5349, https://doi.org/10.1021/acs.chemmater.0c01734.
[16] W. Zhang, H. Zuo, Z. Cheng, Y. Shi, Z. Guo, N. Meng, A. Thomas, Y. Liao, Macroscale Conjugated Microporous Polymers: Controlling Versatile Functionalities Over Several Dimensions, Adv. Mater. 34 (18) (2022) 2104952, https://doi.org/10.1002/adma.202104952.
[17] S. Ma, Z. Li, J. Jia, Z. Zhang, H. Xia, H. Li, X. Chen, Y. Xu, X. Liu, Amide-linked covalent organic frameworks as efficient heterogeneous photocatalysts in water, Chin, J. Catal. 42 (11) (2021) 2010–2019, https://doi.org/10.1016/S1872-2067(21)63836-6.
[18] X. Zhao, P. Pachfule, A. Thomas, Covalent organic frameworks (COFs) for electrochemical applications, Chem. Soc. Rev. 50 (2021) 6871–6913, https://doi.org/10.1039/D0CS01569E.
[19] S. Das, P. Heasman, T. Ben, S. Qiu, Porous Organic Materials: Strategic Design and Structure-Function Correlation, Chem. Rev. 117 (3) (2017) 1515–1563, https://doi.org/10.1021/acs.chemrev.6b00439.
[20] Z. Chang, D.-S. Zhang, Q. Chen, X.-H. Bu, Microporous organic polymers for gas storage and separation applications, PCCP 15 (15) (2013) 5430–5442, https://doi.org/10.1039/C3CP50517K.
[21] W. Wang, M. Zhou, D. Yuan, Carbon dioxide capture in amorphous porous organic polymers, J. Mater. Chem. A 5 (4) (2017) 1334–1347, https://doi.org/10.1039/c6ta09234a.
[22] Q. Sun, B. Aguila, Y. Song, S. Ma, Tailored Porous Organic Polymers for Task-Specific Water Purification, Acc. Chem. Res. 53 (4) (2020) 812–821, https://doi.org/10.1021/acs.accounts.0c00007.
[23] S. Lu, Q. Liu, R. Han, M. Guo, J. Shi, C. Song, N. Ji, X. Lu, D. Ma, Potential applications of porous organic polymers as adsorbent for the adsorption of volatile organic compounds, J. Environ. Sci. 105 (2021) 184–203, https://doi.org/10.1016/j.jes.2021.01.007.
[24] B. Wang, Z. Xie, Y. Li, Z. Yang, L. Chen, Dual-Functional Conjugated Nanoporous Polymers for Efficient Organic Pollutants Treatment in Water: A Synergistic Strategy of Adsorption and Photocatalysis, Macromolecules 51 (9) (2018) 3443–3449, https://doi.org/10.1021/acs.macromol.8b00669.
[25] E. Vitaku, C.N. Gannett, K.L. Carpenter, L. Shen, H.D. Abruña, W.R. Dichtel, Phenazine-Based Covalent Organic Framework Cathode Materials with High Energy and Power Densities, J. Am. Chem. Soc. 142 (1) (2020) 16–20, https://doi.org/10.1021/jacs.9b08147.
[26] Y. Wang, H. Liu, Q. Pan, C. Wu, W. Hao, J. Xu, R. Chen, J. Liu, Z. Li, Y. Zhao, Construction of Fully Conjugated Covalent Organic Frameworks via Facile Linkage Conversion for Efficient Photoenzymatic Catalysis, J. Am. Chem. Soc. 142 (13) (2020) 5958–5963, https://doi.org/10.1021/jacs.0c00923.
[27] D.-H. Yang, Y. Tao, X. Ding, B.-H. Han, Porous organic polymers for electrocatalysis, Chem. Soc. Rev. 51 (2) (2022) 761–791, https://doi.org/10.1039/D1CS00887K.
[28] Y. Chen, Z. Li, R. Ding, T. Liu, H. Zhao, X. Zhang, Construction of porphyrin and viologen-linked cationic porous organic polymer for efficient and selective gold recovery, J. Hazard. Mater. 426 (2022), 128073, https://doi.org/10.1016/j.jhazmat.2021.128073.
[29] S. Yang, T. Li, Y. Cheng, W. Fan, L. Wang, Y. Liu, L. Bian, C.-H. Zhou, L.-Y. Zheng, Q.-E. Cao, Covalent Organic Framework Isomers for Photoenhanced Gold Recovery from E-Waste with High Efficiency and Selectivity, ACS Sustain. Chem. Eng. 10 (30) (2022) 9719–9731, https://doi.org/10.1021/acssuschemeng.2c00285.

[30] H.-L. Qian, F.-L. Meng, C.-X. Yang, X.-P. Yan, Irreversible Amide-Linked Covalent Organic Framework for Selective and Ultrafast Gold Recovery, Angew. Chem. Int. Ed. 59 (40) (2020) 17607–17613, https://doi.org/10.1002/anie.202006535.
[31] L. Zhang, Q.-Q. Zheng, S.-J. Xiao, J.-Q. Chen, W. Jiang, W.-R. Cui, G.-P. Yang, R.-P. Liang, J.-D. Qiu, Covalent organic frameworks constructed by flexible alkyl amines for efficient gold recovery from leaching solution of e-waste, Chem. Eng. J. 426 (2021), 131865, https://doi.org/10.1016/j.cej.2021.131865.
[32] J. Son, Y. Hong, G. Han, T.S. Nguyen, C.T. Yavuz, J.-I. Han, Gold recovery using porphyrin-based polymer from electronic wastes: Gold desorption and adsorbent regeneration, Sci. Total Environ. 704 (2020), 135405, https://doi.org/10.1016/j.scitotenv.2019.135405.
[33] K.S. Song, T. Ashirov, S.N. Talapaneni, A.H. Clark, A.V. Yakimov, M. Nachtegaal, C. Copéret, A. Coskun, Porous polyisothiocyanurates for selective palladium recovery and heterogeneous catalysis, Chem 8 (7) (2022) 2043–2059, https://doi.org/10.1016/j.chempr.2022.05.009.
[34] Y. Hong, D. Thirion, S. Subramanian, M. Yoo, H. Choi, H.Y. Kim, J.F. Stoddart, C. T. Yavuz, Precious metal recovery from electronic waste by a porous porphyrin polymer, Proc. Natl. Acad. Sci. 117 (28) (2020) 16174, https://doi.org/10.1073/pnas.2000606117.
[35] S.-S. Qin, Z.-K. Wang, L. Hu, X.-H. Du, Z. Wu, M. Strømme, Q.-F. Zhang, C. Xu, Dual-functional ionic porous organic framework for palladium scavenging and heterogeneous catalysis, Nanoscale 13 (7) (2021) 3967–3973, https://doi.org/10.1039/D1NR00172H.
[36] T. Li, C. Chen, A.H. Brozena, J.Y. Zhu, L. Xu, C. Driemeier, J. Dai, O.J. Rojas, A. Isogai, L. Wågberg, L. Hu, Developing fibrillated cellulose as a sustainable technological material, Nature 590 (7844) (2021) 47–56, https://doi.org/10.1038/s41586-020-03167-7.
[37] A. Berglund Lars, I. Burgert, Bioinspired Wood Nanotechnology for Functional Materials, Adv. Mater. 30 (19) (2018) 1704285, https://doi.org/10.1002/adma.201704285.
[38] C. Xu, X. Kong, S. Zhou, B. Zheng, F. Huo, M. Strømme, Interweaving metal–organic framework-templated Co–Ni layered double hydroxide nanocages with nanocellulose and carbon nanotubes to make flexible and foldable electrodes for energy storage devices, J. Mater. Chem. A 6 (47) (2018) 24050–24057, https://doi.org/10.1039/C8TA10133G.
[39] S. Zhou, M. Stromme, C. Xu, Highly Transparent, Flexible and Mechanically Strong Nanopapers of Cellulose Nanofibers @ Metal-Organic Frameworks, Chem. Eur. J. 25 (2019) 3515–3520, https://doi.org/10.1002/chem.201806417.
[40] S. Zhou, X. Kong, B. Zheng, F. Huo, M. Strømme, C. Xu, Cellulose Nanofiber @ Conductive Metal-Organic Frameworks for High-Performance Flexible Supercapacitors, ACS Nano 13 (8) (2019) 9578–9586, https://doi.org/10.1021/acsnano.9b04670.
[41] S. Zhou, V. Apostolopoulou-Kalkavoura, M.V. Tavares da Costa, L. Bergström, M. Strømme, C. Xu, Elastic Aerogels of Cellulose Nanofibers@Metal–Organic Frameworks for Thermal Insulation and Fire Retardancy, Nano-Micro Lett. 12 (1) (2020) 9, https://doi.org/10.1007/s40820-019-0343-4.
[42] X. Kong, S. Zhou, M. Strømme, C. Xu, Redox active covalent organic framework-based conductive nanofibers for flexible energy storage device, Carbon 171 (2021) 248–256, https://doi.org/10.1016/j.carbon.2020.09.003.
[43] S. Zhou, Z. Qiu, M. Strømme, C. Xu, Solar-driven ionic power generation via a film of nanocellulose @ conductive metal–organic framework, Energy. Environ. Sci. 14 (2) (2021) 900–905, https://doi.org/10.1039/D0EE02730H.
[44] S. Zhou, X. Kong, M. Strømme, C. Xu, Efficient Solar Thermal Energy Conversion and Utilization by a Film of Conductive Metal-Organic Framework Layered on Nanocellulose, ACS Mater. Lett. 4 (6) (2022) 1058–1064, https://doi.org/10.1021/acsmaterialslett.2c00190.
[45] X. Kong, S. Zhou, M. Strømme, C. Xu, All-cellulose-based freestanding porous carbon nanocomposites and their versatile applications, Compos. B Eng. 232 (2022), 109602, https://doi.org/10.1016/j.compositesb.2021.109602.
[46] X. You, L. Cao, Y. Liu, H. Wu, R. Li, Q. Xiao, J. Yuan, R. Zhang, C. Fan, X. Wang, P. Yang, X. Yang, Y. Ma, Z. Jiang, Charged Nanochannels in Covalent Organic Framework Membranes Enabling Efficient Ion Exclusion, ACS Nano 16 (8) (2022) 11781–11791, https://doi.org/10.1021/acsnano.2c04767.
[47] S. Mitra, S. Kandambeth, B.P. Biswal, A. Khayum M., C.K. Choudhury, M. Mehta, G. Kaur, S. Banerjee, A. Prabhune, S. Verma, S. Roy, U.K. Kharul, R. Banerjee, Self-Exfoliated Guanidinium-Based Ionic Covalent Organic Nanosheets (iCONs), J. Am. Chem. Soc. 138 (8) (2016) 2823–2828, doi:10.1021/jacs.5b13533.
[48] H. Zhang, J. Ma, C. Liu, L. Li, C. Xu, Y. Li, Y. Li, H. Tian, Antibacterial activity of guanidinium-based ionic covalent organic framework anchoring Ag nanoparticles, J. Hazard. Mater. 435 (2022), 128965, https://doi.org/10.1016/j.jhazmat.2022.128965.
[49] H. Yang, L. Yang, H. Wang, Z. Xu, Y. Zhao, Y. Luo, N. Nasir, Y. Song, H. Wu, F. Pan, Z. Jiang, Covalent organic framework membranes through a mixed-dimensional assembly for molecular separations, Nat. Commun. 10 (1) (2019) 2101, https://doi.org/10.1038/s41467-019-10157-5.
[50] Y.S. Ho, G. McKay, Pseudo-second order model for sorption processes, Process Biochem. 34 (5) (1999) 451–465, https://doi.org/10.1016/S0032-9592(98)00112-5.
[51] J.D.S. Newman, G.J. Blanchard, Formation of Gold Nanoparticles Using Amine Reducing Agents, Langmuir 22 (13) (2006) 5882–5887, https://doi.org/10.1021/la060045z.